Experimental investigation and flow analysis of clear-water scour around pier and abutment in proximity

Water Science and Engineering 2023, 16(1): 94−105

HOSTED BY

ELSEVIER

Available online at www.sciencedirect.com

Water Science and Engineering

journal homepage: wse.hhu.edu.cn

Experimental investigation and flow analysis of clear-water scour around pier and abutment in proximity

Mohammad Saeed Fakhimjoo [a], Abdollah Ardeshir [a], Kourosh Behzadian [b,*], Hojat Karami [c]

[a] *Department of Civil and Environmental Engineering, Amirkabir University of Technology, Tehran 15875-4413, Iran*
[b] *School of Computing and Engineering, University of West London, London W5 5RF, UK*
[c] *Department of Civil Engineering, Semnan University, Semnan 35131-19111, Iran*

Received 27 April 2022; accepted 14 November 2022
Available online 6 December 2022

Abstract

Local scour around bridge piers and abutments is one of the most significant causes of bridge failure. Despite a plethora of studies on scour around individual bridge piers or abutments, few studies have focused on the joint impact of a pier and an abutment in proximity to one another on scour. This study conducted laboratory experiments and flow analyses to examine the interaction of piers and abutments and their effect on clear-water scour. The experiments were conducted in a rectangular laboratory flume. They included 18 main tests (with a combination of different types of piers and abutments) and five control tests (with individual piers or abutments). Three pier types (a rectangular pier with a rounded edge, a group of three cylindrical piers, and a single cylindrical pier) and two abutment types (a wing−wall abutment and a semi-circular abutment) were used. An acoustic Doppler velocimeter was used to measure the three-dimensional flow velocity for analyses of streamline, velocity magnitude, vertical velocity, and bed shear stress. The results showed that the velocity near the pier and abutment increased by up to 80%. The maximum scour depth around the abutment increased by up to 19%. In contrast, the maximum scour depth around the pier increased significantly by up to l71%. The presence of the pier in the vicinity of the abutment led to an increase in the scour hole volume by up to 87% relative to the case with a solitary abutment. Empirical equations were also derived to accurately estimate the maximum scour depth at the pier adjacent to the abutment.

Keywords: Abutment; ADV; Bridge scour; Laboratory experiment; Maximum scour depth; Pier

1. Introduction

Bridge scour is the erosion of streambeds or removal of bank materials from bridge foundations (Mays, 2001). Scour at bridge piers and abutments is recognised as one of the most frequent causes of bridge failure, leading to substantial damage to transportation infrastructure (Kumcu et al., 2014). Scour is the main cause of more than 60% of all bridge failures in the United States (Abid, 2017; Saha et al., 2018) and 70% in the United Kingdom (Lamb et al., 2019). Previous studies have proven that the scouring mechanisms are similar at bridge piers and abutments (Melville, 1997). When approaching flow hits the upstream side of piers and abutments, stagnation pressure is created due to the flow velocity that decreases through flow depth, causing a downflow. The resulting downflow forms horizontal horseshoes and vertical wake vortices that are the main causes of local erosion (Hamill, 2011).

Scour around river structures has attracted the attention of many researchers in this field (Karami et al., 2011). Melville and Raudkivi (1977) were among the first to analyse the flow characteristics around a cylindrical pier at the scour hole. They observed that the location of the maximum shear stress was where the scour first occurred. As with the horseshoe

* Corresponding author.
E-mail address: kourosh.behzadian@uwl.ac.uk (Kourosh Behzadian).
Peer review under responsibility of Hohai University.

https://doi.org/10.1016/j.wse.2022.12.001

vortex at bridge piers, primary vortex at bridge abutments is responsible for the scour hole growth. Coleman et al. (2003) studied scour development at a bridge abutment and developed a new formula for estimating scour at the abutment based on flow depth, abutment size, and flow intensity. Some studies have specifically focused on the scour depth caused by different shapes of piers or abutments (Melville, 1997; Melville and Coleman, 2000; Fael et al., 2016). More recently, Fael et al. (2016) introduced a shape factor (k_s) for the scour depth of different pier shapes relative to the single-cylinder pier scour depth. Melville (1997) previously suggested shape factor values of 0.75 for wing-walls and 0.45 to 0.60 for spill-through abutments.

Multiple studies have produced empirical equations for estimating the local scour depth at piers and abutments (Froehlich, 1988; Melville, 1997; Richardson and Davis, 2001; Sheppard and Miller, 2006; Sheppard et al., 2014). Sheppard et al. (2014) evaluated 23 commonly used scour prediction equations with laboratory and field data. A new equation that obtained the least total error was proposed by melding and slightly modifying the equations of Sheppard and Miller (2006) and Melville (1997). However, the difference in the maximum scour depth predictions using different empirical equations was about 100%, indicating that new equations need to be developed (Pizarro et al., 2020).

Flow field analysis could provide better insight into the scouring process. Dey and Barbhuiya (2005b) measured the turbulent flow field around a short rectangular abutment using the acoustic Doppler velocimeter (ADV). Pasupuleti et al. (2022) investigated flow characteristics and velocity field around circular piers in different layouts. They observed that flow separation occurred behind upstream piers, and a primary vortex was generated due to the downflow in front of the upstream pier. Guan et al. (2019) presented principal characteristics of the horseshoe vortices and turbulent flow fields at a circular bridge pier when a scour hole was developing. They observed that the horseshoe vortices were also enlarged, strengthened, and reproduced as the scour hole grew, and the location of the core of the main horseshoe vortex was asymptotically stabilised after 24 h. Yang et al. (2020) observed that of the three pressure flow types (free surface flow, submerged office flow, and overtopping flow), submerged orifice flow had the highest velocity intensity, whereas free surface flow had the lowest. Melville et al. (2021) studied the effect of streamwise abutment length on the scour and turbulence flow at a contraction section. They observed that the long contraction abutment caused most of the turbulent zone to move to the downstream abutment, and an equilibrium scour hole formed downstream.

Many studies have focused on the scour at individual piers or abutments. However, few have addressed the interaction of scour piers and abutments. Hong (2005) studied the interaction between local pier scour and contraction scour around a bridge pier and showed that the presence of a pier in the contracted flow area reduced the contraction scour depth by 25%. After scouring, flow redistribution at greater depths can also reduce the flow velocity and decrease the scour depth (Hong and Abid, 2016). Oben-Nyarko and Ettema (2011) performed laboratory experiments to clarify the impact of the interaction between a pier and an abutment (spill-through or wing-wall shape) on the scour depth and found that a pier close to an abutment had a minor influence on the maximum scour depth around the abutment. On the contrary, the scour depth around the pier can increase significantly as compared to the situation around a solitary pier. Saha et al. (2018) showed that the presence of a pier near an abutment had no impact on the location of scour but slightly decreased the maximum scour depth. Khajeh and Vaghefi (2020) showed that the maximum scour depth around an abutment in proximity to an inclined pier in a river bend occurred at the upstream side of the outer abutment. However, the impact of the distance between the pier and abutment was not analysed.

Although many studies have focused on the bridge scour at an individual pier or abutment, few studies have focused on the interaction between a pier and nearby abutment. In addition, during this interaction, the scour depth can be significantly affected by the shapes of the pier and abutment. Therefore, further experimental tests are needed, and new relations should be derived. The flow field, velocity, and streamline during this interaction should be analysed as well. To the best of the authors' knowledge, little information is currently available on how a pier near an abutment affects the scour depth and flow characteristics at both piers and abutments. Therefore, this study aimed to conduct laboratory experiments, analyse streamlines, and derive new empirical equations on the effect of interaction between bridge piers and abutments on the scour depth and flow field. This study also aimed to analyse the impacts of the shape and layout of piers and abutments and their distance on the scour depth. To achieve these goals, three-dimensional (3D) flow characteristics were investigated using ADV measurements. Flow streamlines, velocities, and bed shear stress were also analysed during the experimental tests to explain the scouring processes around piers and abutments.

2. Materials and methods

All experiments in this study were conducted using a rectangular laboratory flume that was 14 m long, 1 m wide, and 1 m high. Fig. 1 shows the schematic side view

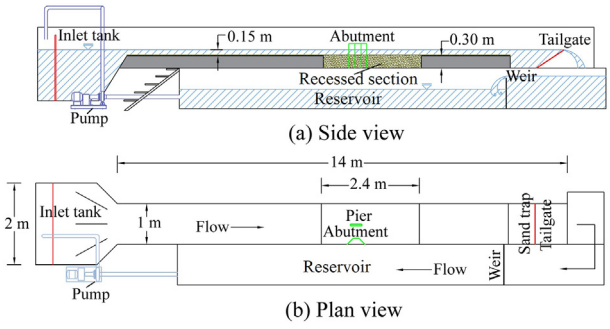

Fig. 1. Schematic side view and plan view of laboratory flume.

(longitudinal section) and plan view of the flume with all dimensions. An actual picture of the flume and its accessories are shown in Fig. A.1. Abutments and piers were placed in the flume far away from the channel entrance (i.e., 6 m downstream the entrance). In this way, a uniform flow was established in the test region, and fully turbulent flow was developed as per the equation suggested by Kirkgöz and Ardiçlioğlu (1997). Uniform sand with a median size of $d_{50} = 0.88$ mm and a geometric standard deviation of $\sigma_g = 1.3\sqrt{d_{84}/d_{16}}$ (with d_{84} and d_{16} denoting the sediment particle diameters at 84% and 16% quantile levels, respectively) was used as the uniform bed material throughout the flume. A recessed section with a length of 2.4 m was provided as the test region. The thickness of the sand layer (bed material) was 30 cm in the recessed section and 2 cm along the rest of the flume. The hydraulic characteristics and procedure of the tests are explained in Appendix A.

Two types of abutments and three types of piers, all made of transparent plexiglass at laboratory scales, were used in the experiments. Fig. 2 shows the following shapes and groups of piers and abutments: a rectangular pier with a rounded edge (R), a group of three cylindrical piers (G), a single cylindrical pier (S), a wing-wall abutment (W), and a semi-circular abutment (C). To remove the impact of the flume sidewall on the scour, Chiew and Melville (1987) suggested that the ratio of the pier diameter (D) to the channel width (B) should be less than 0.1 ($D/B < 0.1$). Moreover, if the ratio of the flow depth (H) to the pier diameter (D) is greater than 3 ($H/D > 3$), the flow depth effect on the scour can be neglected (Chiew, 1995). According to Ettema (1980), if the pier diameter relative to the sediment mean diameter is greater than 50, sediment size has no impact on the scour. Therefore, a pier diameter of 5 cm was selected to remove the effects of sidewall, sediment size, and flow depth on the scour. The abutments were short, with lengths (L_a) less than the flow depth (H) ($L_a/H < 1$). Thus, the scour depth was independent of the flow depth, according to Melville (1992) and Melville and Raudkivi (1977).

According to dimensional analysis using the Buckingham theorem, the local scour around a pier or an abutment is a function of different non-dimensional variables:

$$f\left(\frac{d_s}{D}, \frac{U}{U_{cr}}, \frac{D}{d_{50}}, \frac{L_a}{D}, \frac{B_a}{D}, \frac{X}{D}, K_{sa}, K_{sp}, \sigma_g, \frac{U}{\sqrt{gD}}, \frac{\rho_s}{\rho}, \frac{Ut}{D}, s, \frac{U\rho D}{\mu}, \frac{H}{D}\right) = 0 \quad (1)$$

where d_s is the scour depth; U is the mean flow velocity; U_{cr} is the critical flow velocity; L_a is the abutment length perpendicular to the flow direction; B_a is the abutment width; X is the distance between the pier and abutment; K_{sa} is the abutment shape factor; K_{sp} is the pier shape factor; g is the gravitational acceleration; ρ_s is the bed material density; ρ is the density of water; t is the time; s is the flume slope; and μ is the water dynamic viscosity. Given that this study mainly focused on the interaction of scour between the pier and abutment, considering the effects of their shapes and distance from one another, all variables were set as constant except for X/D, K_{sa}, K_{sp}, and d_s/D, which were varied to determine the effects of the shape and the distance between the pier and abutment.

The first group of experiments included five control tests in which individual piers or abutments were used as benchmarks. The control tests were compared with eighteen main tests in which piers and abutments were placed together. Table 1 lists the information and results of all experiments (23 tests). Control tests are designated with a T and main tests are designated with an S, followed by the acronyms defined above for the pier and abutment shapes and groups. Main tests were conducted with three different distances between the pier and abutment (X as defined in Fig. 2(f)) for each shape combination. X values were set as 1.5, 3.0, and 6.0 times the pier diameter (D), and denoted by *1*, *2*, and *3* in the test names, respectively. Based on several trial runs of the control tests, the run time of all 18 main tests was set as 27 h during which the scour depth was equal to or greater than 80% of the maximum scour depth. The actual

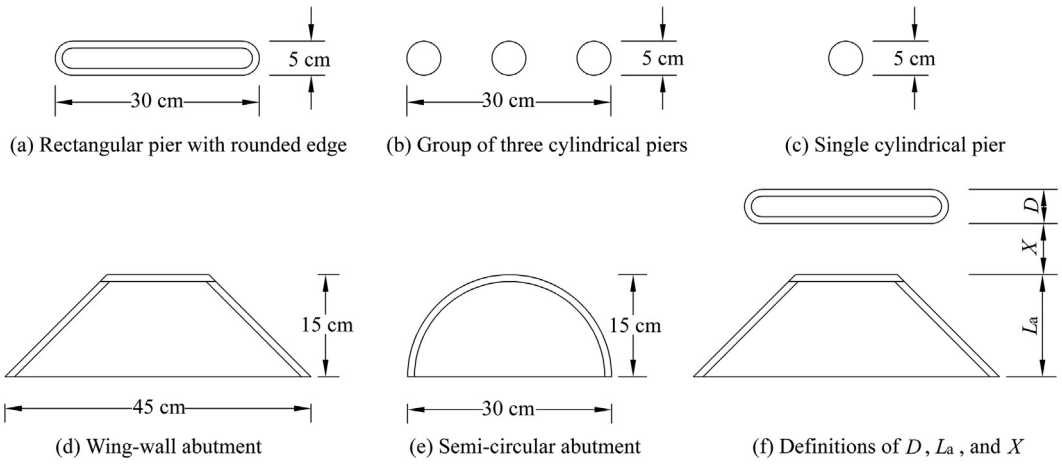

Fig. 2. Schematic representation of different shapes and dimensions of piers and abutments used in tests.

Table 1
Information and results of laboratory experiments.

Test category	Test No.	Test name	*X/D*	Observed relative maximum scour depth		Estimated relative maximum scour depth		Scour volume (cm^3)
				Abutment	Pier	Eq. (3)	Eq. (4)	
Control test	1	TW		3.4				26 954
	2	TC		3.6				26 474
	3	TS			1.66			3 560
	4	TG			1.96[a], 1.74[b], 1.56[c]			8 283
	5	TR			1.46			3 554
Main test (pier combined with wing-wall abutment)	6	SWS3	6.0	3.30	2.46	2.48*	2.40*	34 477
	7	SWG3	6.0	3.20	2.22[a], 1.92[b], 1.68[c]	2.78*	2.43*	35 630
	8	SWR3	6.0	3.42	2.04	2.28*	2.25*	31 199
	9	SWS2	3.0	3.52	2.62	2.79*	2.69*	31 102
	10	SWG2	3.0	3.40	2.94[a], 2.24[b], 1.90[c]	3.09*	2.72*	42 035
	11	SWR2	3.0	3.30	2.68	2.59*	2.52*	29 832
	12	SWS1	1.5	3.92	4.22	3.76*	4.21*	49 535
	13	SWG1	1.5	3.92	4.20[a], 4.26[b], 3.28[c]	4.06*	4.25*	48 751
	14	SWR1	1.5	3.40	3.96	3.56*	3.94*	37 673
Main test (pier combined with semi-circular abutment)	15	SCS3	6.0	3.50	2.12	2.48*	2.11*	32 622
	16	SCG3	6.0	3.86	2.22[a], 1.94[b], 1.70[c]	2.78*	2.13*	43 287
	17	SCR3	6.0	3.64	2.10	2.28*	1.97*	33 372
	18	SCS2	3.0	3.80	2.32	2.79*	2.36*	32 352
	19	SCG2	3.0	3.90	2.28[a], 2.48[b], 2.00[c]	3.09*	2.38*	47 183
	20	SCR2	3.0	3.76	2.12	2.59*	2.21*	32 471
	21	SCS1	1.5	3.78	3.80	3.76*	3.69*	36 306
	22	SCG1	1.5	4.30	3.80[a], 4.10[b], 3.02[c]	4.06*	3.73*	45 756
	23	SCR1	1.5	3.90	3.54	3.56*	3.46*	38 143

Note: Data with the superscripts "a", "b", and "c" are the observed relative maximum scour depths at the first, second, and third piers in the group of three cylindrical piers, respectively; and data with the superscript "*" are the estimated maximum scour depth at the first pier in the group of three cylindrical piers.

equilibrium time was around 10%−20% longer than this run time. However, given the long period of time required to achieve equilibrium as per the recommendation of Dey and Barbhuiya (2005a), a 27-h duration for each test was set as the time required to reach more than 80% of the equilibrium scour depth based on a large number of main tests. A detailed description of the temporal evolution of the scour depth in the control and main tests is provided in Appendix A. The maximum scour depths at a pier and abutments (d_{sp} and d_{sa}, respectively) were assigned as the depths of the scour holes at piers and abutments at the end of each test.

At the end of each test, water was carefully drained off from the flume to ensure that no disturbance occurred in the scour hole region. Afterwards, the maximum scour depth and bed geometry were measured using a laser meter with an accuracy of ±1.5 mm. In 3D velocity measurement experiments, bed materials were fixed by spraying resin to prevent any scouring, and a 25-Hz SonTek ADV was used to measure the 3D flow velocity on a flat fixed bed. A total of 1 700 points with distances from 1 to 10 cm were measured at five different depths. The location and spacing of the velocity measurement points are shown in Fig. A.2.

3. Results and discussion

3D flow characteristics of the main tests were analysed. The impacts of a pier and abutment in proximity to one another on the maximum scour depth at the abutment and piers were discussed separately. These impacts were also analysed in terms of scour hole characteristics and the relationship between scour volume and cross-section. Several empirical equations for prediction of the scour depth at a pier near an abutment were derived from experiments. The effect of a pier and abutment in proximity to one another on the temporal evolution of the scour hole is also discussed in Appendix A.

3.1. Streamline analysis

Fig. 3 shows the near-bed ($z/H = 0.033$ with z denoting the depth of the flow velocity measurement) streamlines for an individual pier, an individual abutment, and a pier and an abutment in proximity to one another with $X/D = 3.0$. As shown in Fig. 3(b), the streamlines around the individual abutment tended to bend leftward, reaching the abutment upstream. After passing through the abutment, flow separation started at the downstream edge of the abutment. A vortex formed in the abutment wake region with a core located at $x/L_a = 1.83$ and $y/L_a = 0.5$ (with x and y denoting Cartesian coordinates in the flow direction and the perpendicular direction, respectively; the origin of the coordinate system is at the right endpoint of the abutment centreline) immediately downstream the abutment, and the streamlines inclined to the left because of the high transverse velocity. These deviated streamlines were visible across the half width of the flume. As

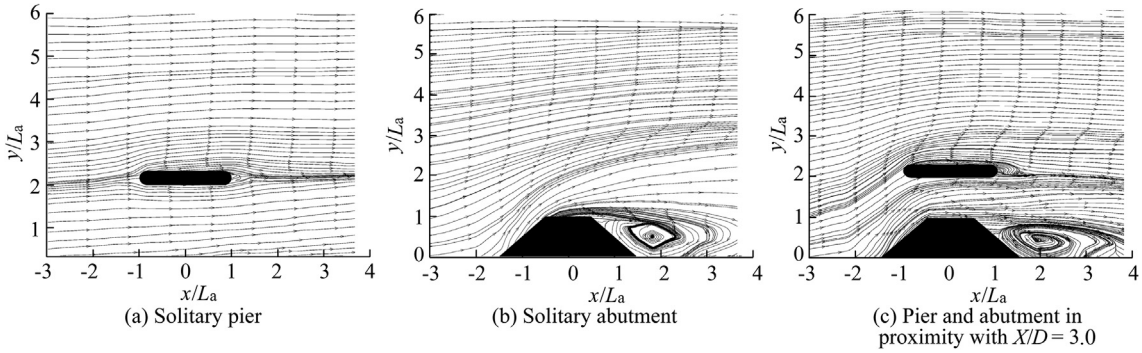

Fig. 3. Near-bed ($z/H = 0.033$) streamlines for (a) solitary pier, (b) solitary abutment, and (c) pier and abutment in proximity with $X/D = 3.0$.

shown in Fig. 3(c), the streamlines were more aligned streamwise when the pier was located near the abutment. After bending to the left facing the abutment, the streamlines met the pier and turned again in the streamwise direction. On the other hand, the presence of the pier channelised the flow between the pier and the abutment. Hence, few streamlines could reach the flume mid-line. The location of the wake vortex core was the same as in the case with the individual abutment. It still had a small width perpendicular to the flow due to the confining effect of the pier downstream of the abutment region. The presence of the pier caused the flow separation to move to the right from the downstream edge of the abutment.

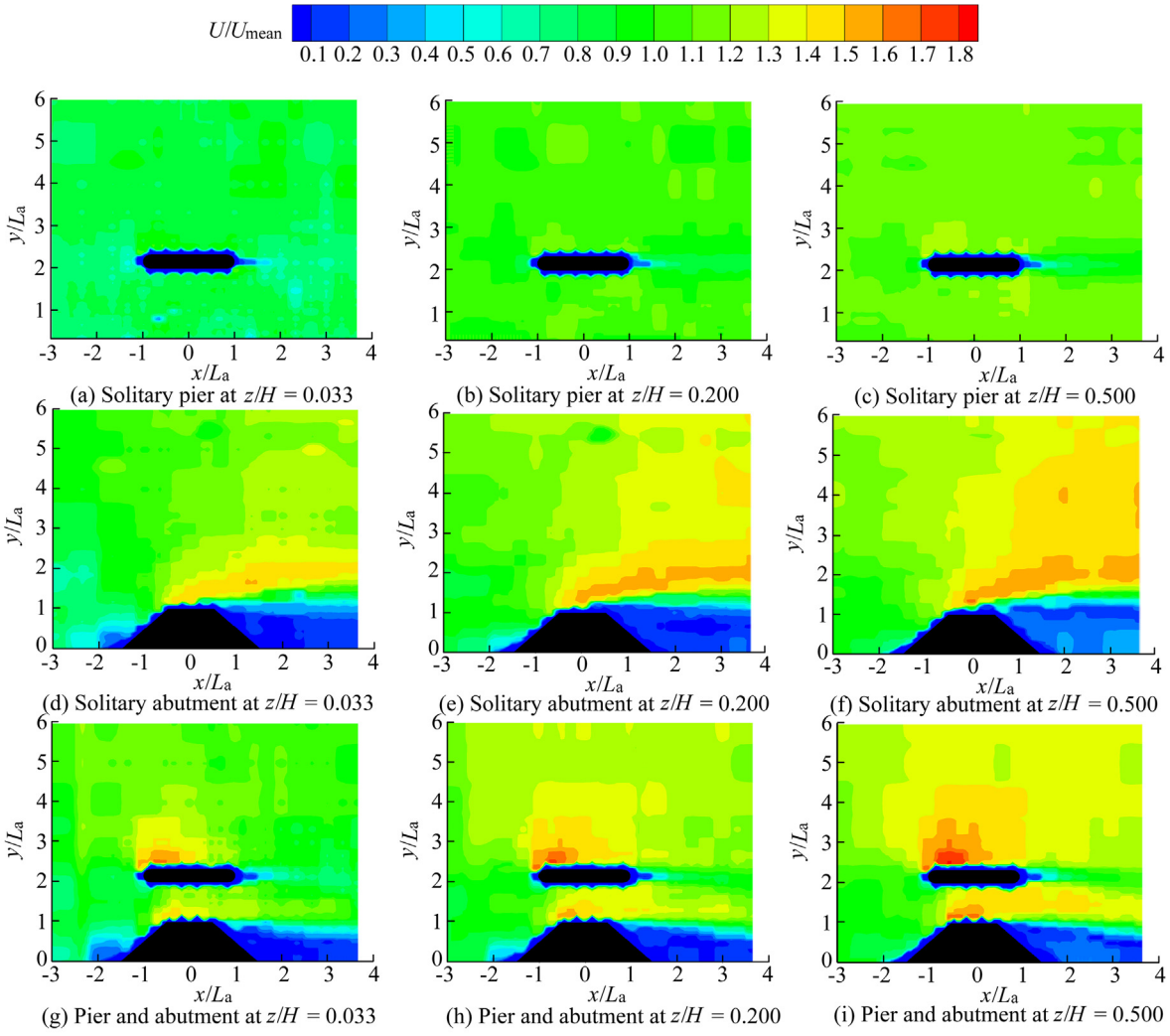

Fig. 4. Time-averaged velocity relative to upstream mean velocity (U/U_{mean}) in different tests and at different depths.

3.2. Velocity magnitude

Fig. 4 shows the velocity magnitudes relative to the upstream mean velocity (U_{mean}) at different depths ($z/H = 0.033$, 0.200, and 0.500). The flow velocity in the case with a solitary pier showed no significant change and was close to the mean velocity in most of the flume area (Figs. 4(a) through (c)). On the near-bed plane ($z/H = 0.033$), the solitary pier increased the velocity by no more than 6% (with a maximum U/U_{mean} of 1.06). When the height for flow velocity measurements was increased, the velocity magnitude was found to increase by 30%. In contrast, in the case with a solitary abutment, the velocity magnitudes increased by 52% on the near-bed plane (Fig. 4(d)) and by 61% at $z/H = 0.500$ (Fig. 4(f)). When the pier and abutment were both in place, the velocities increased by 62% on the near-bed plane (Fig. 4(g)) and by 80% at $z/H = 0.500$ (Fig. 4(i)). Due to the protruding abutment and flow contraction, a high-velocity region formed at the upstream edge of the individual abutment, developed downstream, and leaned to the left (Figs. 4(d) through (f)). In the case with a pier and an abutment in proximity to one another, two high-velocity regions (Figs. 4(g) through (i)) formed on the upstream right side of the pier and at the upstream abutment edge, respectively. As discussed in Section 3.1, a high-velocity zone was established between the pier and abutment, causing the detached shear layer to contract. Compared to the case with a solitary abutment, the wake region and reverse flow were compacted in the case with a pier and an abutment in proximity to one another. Furthermore, the high-velocity region expanded significantly in the flume and might have produced a wide scour hole. The velocity magnitude was higher on the left side of the pier than at the solitary pier due to the higher transverse velocity with $U/U_{mean} = 1.8$.

3.3. Vertical velocity

Fig. 5 shows the contours of the relative vertical velocity (the ratio of the near-bed vertical velocity (w) to the flow mean velocity). The downflow upstream of the pier (Fig. 5(a)) was responsible for the generation of the horseshoe vortices digging the scour hole. In the wake region of the solitary pier, high vertical velocity in the upward direction indicated that the wake vortices moved away the bed materials. Similarly, the downflow across the upstream edge of the solitary abutment (Fig. 5(b)) showed that the primary vortices were the main cause of the scour around the abutment. According to Fig. 5(c), the downflow and primary vortices were stronger when the pier was located at $X/D = 3.0$ than in the cases with a solitary pier and a solitary abutment. The maximum relative downflow velocities were −0.15 for the solitary pier, −0.19 for the solitary abutment, and −0.21 for the pier and abutment in proximity to one another. The primary vortices for the abutment that extended over the left upstream of the pier were the predominant cause of the scour at the pier. In addition, the flow structure around the pier was completely changed, leading to a scour hole that was different from that in the case with the solitary pier.

3.4. Bed shear stress

The scouring of bed materials is basically attributed to the bed shear stress. A bed shear stress that exceeds the critical shear stress can cause bed materials to move. Hence, the bed shear stress was analysed to investigate the relationship between the scour phenomena and the bed shear stress as a principal parameter of scour. The bed shear stress can be estimated using the near-bed shear stress obtained from the measured 3D flow velocities. The mean bed shear stress (τ) on the fixed-bed plane was calculated by the following equation used by Dey and Barbhuiya (2005b) and Zhang et al. (2021) with $z/H = 0.033$:

$$\tau = \sqrt{\tau_x^2 + \tau_y^2} \tag{2}$$

where τ_x and τ_y are the mean bed shear stresses in the x and y directions, respectively, with $\tau_x = -\rho(\overline{u'v'} + \overline{u'w'})$ and $\tau_y = -\rho(\overline{v'u'} + \overline{v'w'})$, where u', v', and w' are the longitudinal, lateral, and vertical velocity fluctuations, respectively. Fig. 6 shows the calculated near-bed shear stresses relative to the critical bed shear stress for the cases with the solitary pier, solitary abutment, and pier R located at $X/D = 3.0$ near abutment W. The critical bed shear stress ($\tau_{cr} = 0.466$ Pa) was

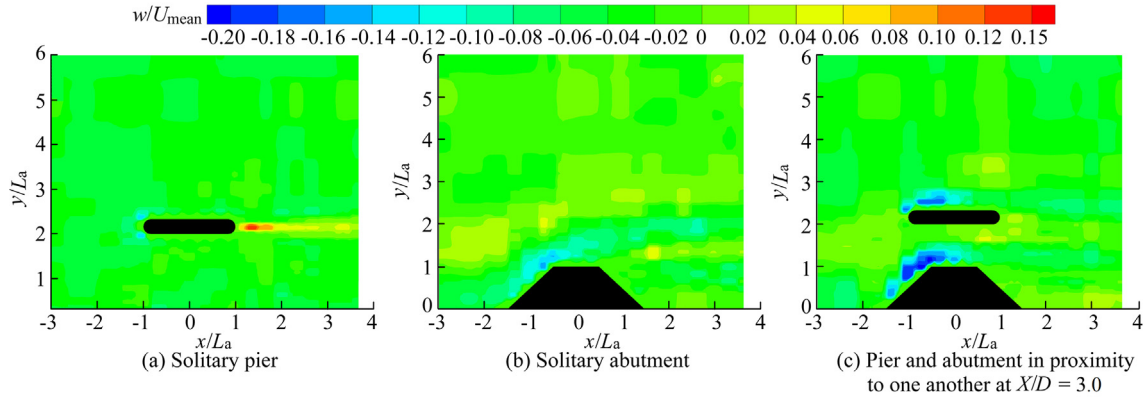

Fig. 5. Distributions of relative vertical velocities (w/U_{mean}) at $z/H = 0.200$ for (a) solitary pier, (b) solitary abutment, and (c) pier and abutment in proximity to one another at $X/D = 3.0$ (with positive w value denoting velocity in upward direction).

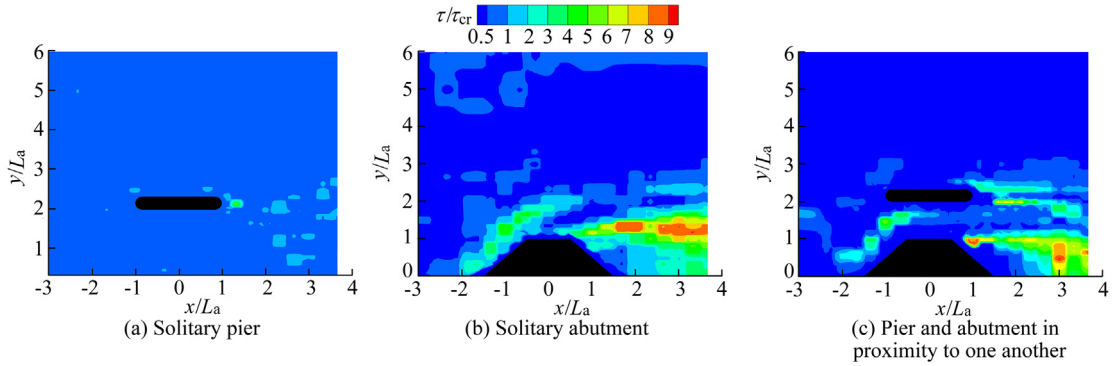

Fig. 6. Relative near-bed shear stresses at $z/H = 0.033$ for tests: (a) solitary pier, (b) solitary abutment, and (c) pier and abutment in proximity to one another.

calculated using the Shields parameter approach. According to Fig. 6(a), τ was far from τ_{cr} in most areas of the test field. In the case of the individual wing-wall abutment, τ increased significantly upstream of the abutment. In a region with an area of about $0.85L_a \times 3L_a$, the bed shear stress exceeded the critical value and reached a maximum value of $4.85\tau_{cr}$ at $x/L_a = -1$ and $y/L_a = 1.31$ (Fig. 6(b)). As shown in Fig. 6(c), locating the pier near the abutment also caused a significant increase in the bed shear stress, but the region with high bed shear stress shrunk to an area of approximately $0.5L_a \times 2L_a$, and the maximum bed shear stress decreased to $3.83\tau_{cr}$ at $x/L_a = -1$ and $y/L_a = 1.31$. Both in cases with a solitary abutment and in those with a pier and an abutment in proximity to one another, the location of the maximum bed shear stress was near the upstream edge of the abutment where the scour process first started and the maximum scour depths were recorded.

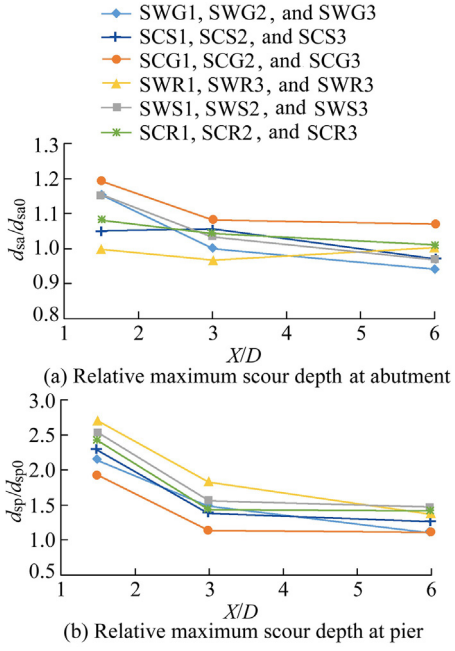

Fig. 7. Relative maximum scour depth at abutment for various combinations of pier and abutment (a) and relative maximum scour depth at pier for various combinations of pier and abutment (b).

3.5. Effect of X/D on maximum scour depth around abutment

Fig. 7(a) shows the variation of the relative maximum scour depth at the abutment (d_{sa}/d_{sa0}, with d_{sa} and d_{sa0} denoting the maximum scour depths around an abutment in the main tests and control tests, respectively) versus X/D with the three shapes of piers in proximity to an abutment. The scour depth slightly decreased as the distance between the piers and the abutment increased. More specifically, when X/D was 1.5 in the cases using piers S and G, d_{sa} at the wing-wall abutment was 15% greater than that in test TW with no pier. In contrast, no significant change was observed in the case using pier R. The maximum scour depth was 19% higher in test SCG1 than in test TC. Nevertheless, d_{sa} increased by approximately 1%−7% in other cases with large X/D values (Table 1). These results

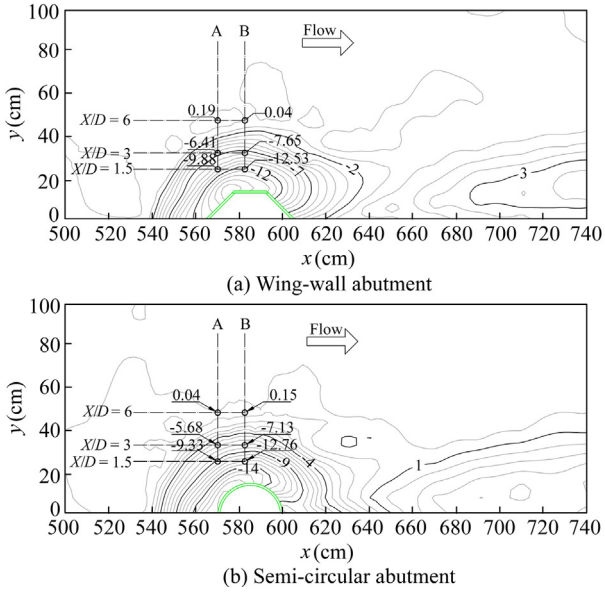

Fig. 8. Scour topographies of control tests for (a) wing-wall abutment and (b) semi-circular abutment (circles represent the locations of maximum scour depth at piers in main tests, dashed line A denotes the location of the upstream head of the rounded rectangular pier and the group of three piers, and dashed line B stands for the location of the upstream head of the single cylindrical pier).

indicated that the pier in proximity to the abutment did not lead to a substantial increase of d_{sa} in the cases with $X/D > 3.0$. As shown in Figs. 4 and 5, the maximum flow velocity around the abutment with a nearby pier was similar to that around a solitary abutment. Thus, a similar scour depth was expected when a pier was placed nearby. These results agreed with the findings of Oben-Nyarko and Ettema (2011) on long wing-wall and spill-through abutments and a rectangular pier. They reported a marginal increase of the abutment scour depth by 5%−7%. They also reported increasing abutment scour depths in some situations and slightly decreasing scour depth in others. When the pier was very close to the abutment ($X/D = 1.5$), the horseshoe and wake vortices induced by the pier strengthened the abutment scour process. When the distance between the pier and abutment increased, the flow field around the pier slightly changed the flow field around the abutment, indicating a minor impact of the pier (Fig. 3). Abid (2017) also found a difference of ±15% between the scour depth around an abutment with a nearby pier and the scour depth around a solitary abutment. This slight difference in scour depth was found in the case with $X/D \geq 3.0$. However, in the case with $X/D = 1.5$, the G pier and the abutment jointly obstructed the flow with a longer obstacle in front of the flow and stronger vortices, leading to a deeper scour hole. Rahimi et al. (2021) reported a 31% increase in the scour depth around a vertical wall abutment when a circular pier was at $X/D = 1.7$, but the scour depth only increased by less than 10% in the case with $X/D > 3.0$.

3.6. Effect of X/D on maximum scour depth around pier

Fig. 7(b) shows the relative maximum scour depth around the pier (d_{sp}/d_{sp0}, with d_{sp} and d_{sp0} denoting the maximum scour depths around the pier in the main tests and control tests, respectively) versus X/D for various combinations of pier and abutment. Unlike the scour around the abutment, the presence of the pier in the proximity of the abutment significantly influenced d_{sp}. With $X/D = 1.5$, d_{sp} in the main test SWR1 was 2.71 times d_{sp0} in the control test TR. The difference in the maximum scour depth was significantly greater than in the case with longer distances between the pier and abutment (i.e., $X/D \geq 3.0$). This indicated that when a pier was placed in the influence region of the abutment scour hole, the scour depth around the pier was highly affected, and its value was similar to the scour depth around the abutment. The impact was evident at piers R and S with a short relative distance (i.e., $X/D = 1.5$). Rahimi et al. (2021) conducted an experiment with a single circular pier and a nearby vertical abutment

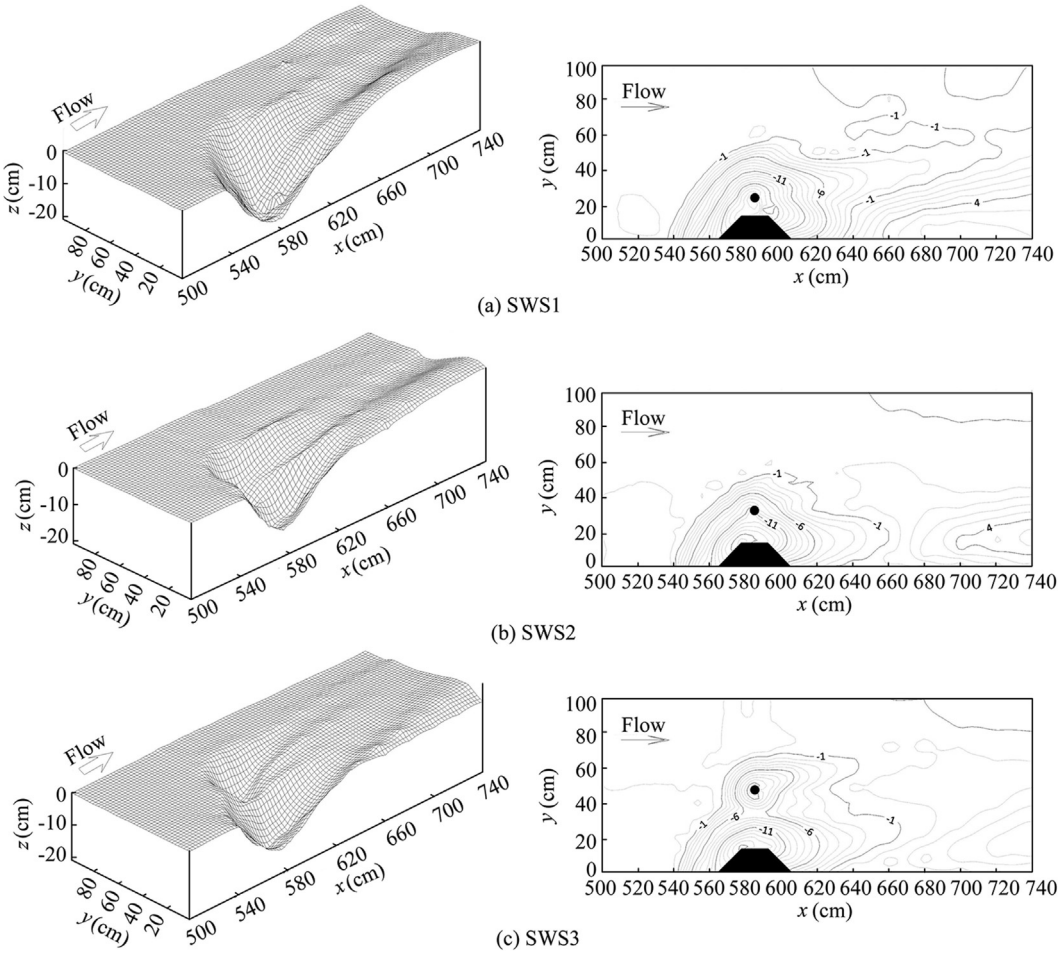

Fig. 9. 3D views and contours of scour hole topographies of main tests SWS1 (a), SWS2 (b), and SWS3 (c).

and reported only a 31% increase in the maximum scour depth around the pier for $X/D = 1.65$, which was much lower than the results of this study and of Oben-Nyarko and Ettema (2011). Further analysis on the scour depth around the pier is provided in Appendix A.

3.7. Analysis of scour holes

Analysis of the scour holes can help us to better understand the physical processes of the scour mechanisms and estimate the maximum scour depth. Fig. 8 shows the scour topography of the control tests using semi-circular and wing-wall abutments after 27 h. The maximum scour depths were at the upstream edge of the wing-wall abutment and with an angle of 35°−40° to the flow direction for the semi-circular abutment. Dey and Barbhuiya (2005a) reported similar results with angles of 45° for the wing-wall abutment and 40°−50° for the semi-circular abutment. The primary vortices that were created upstream of the abutment controlled the location of the maximum scour depth at the upstream edge of the abutment. In the cases with a pier and an abutment in proximity to one another, the locations of these vortices did not change. Thus, the location of the maximum scour depth around the abutment did not change.

Fig. 9 shows 3D views and contours of the scour hole topographies when pier S was at different distances from abutment W. With $X/D = 6.0$ (i.e., SWS3), two distinct scour holes, one around the pier and another around the abutment, were observed. Table 1 shows the scour volume, defined as the difference between the volume of the conical scour hole and the initial bed surface level, for all tests. These data demonstrate that a pier placed in the vicinity to an abutment resulted in a 12%−87% increase of the scour hole volume relative to that in the case using a solitary abutment. The increase of the scour hole volume did not significantly affect the maximum scour depth around the abutment in the main tests. Therefore, the presence of the pier in the influence region of the scour hole around the abutment had an insignificant influence on d_{sa} but significantly affected the extent of the scour hole (Fig. 10).

Fig. 10 shows the lateral cross-sections of the scour holes for the maximum scour depths around the pier and abutment (i.e., at reach lengths of 570.0 cm and 582.5 cm in the flume that corresponded to sections A and B in Fig. 8, respectively)

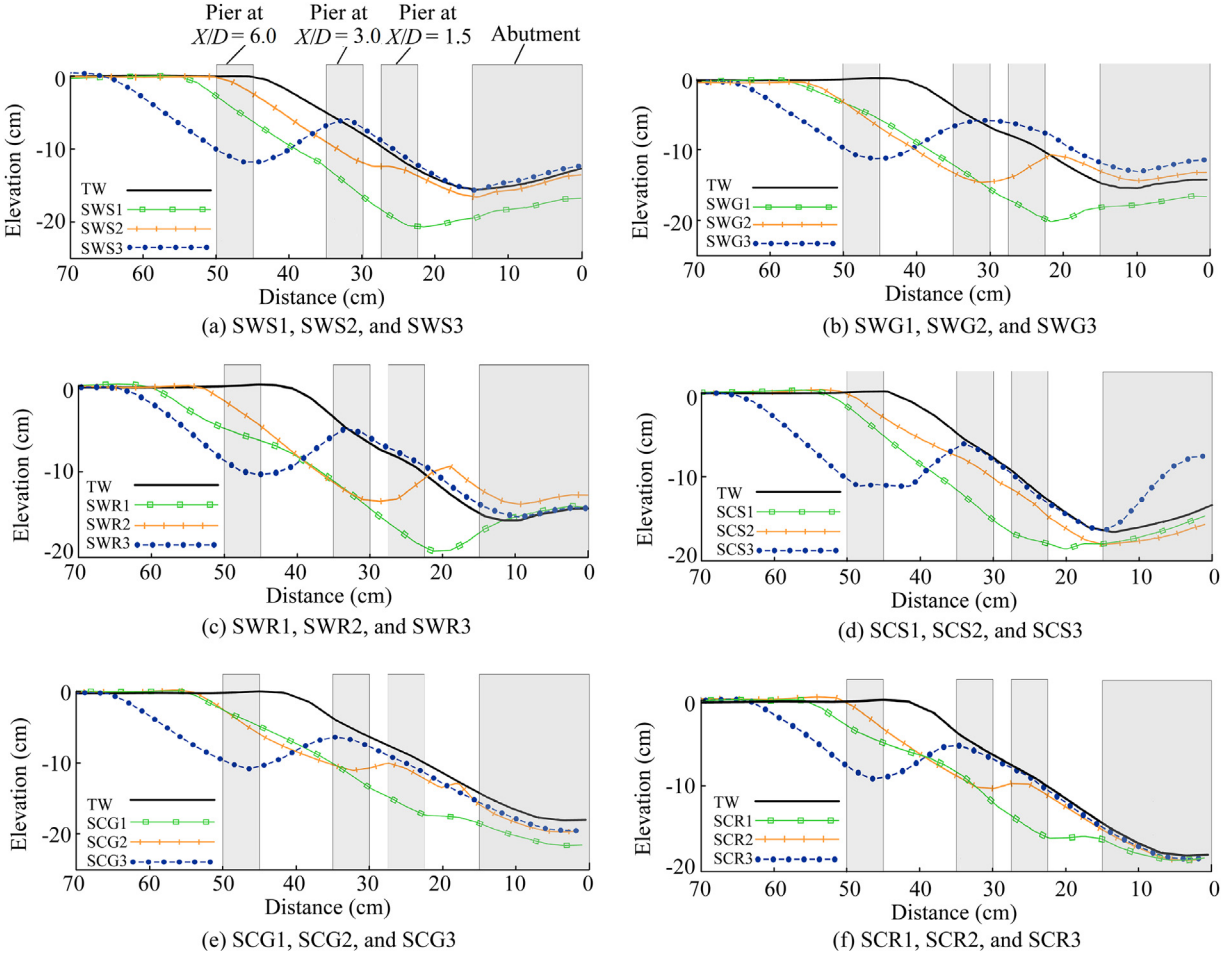

Fig. 10. Lateral cross-sections of scour holes for maximum scour depths around pier and abutment (at longitudinal reaches of $x = 570.0$ cm and 582.5 cm) with different relative distances from abutment ($X/D = 1.5$, 3.0, and 6.0) for main tests: (a) SWS1, SWS2, and SWS3; (b) SWG1, SWG2, and SWG3; (c) SWR1, SWR2, and SWR3; (d) SCS1, SCS2, and SCS3; (e) SCG1, SCG2, and SCG3; and (f) SCR1, SCR2, and SCR3.

with different pier distances (i.e., 22.5 cm for $X/D = 1.5$, 30.0 cm for $X/D = 3.0$, and 45.0 cm for $X/D = 6.0$). The abutment control tests showed that almost no scour occurred in the area $6D$ away from the abutment, and the scour hole around the abutment was almost unchanged. However, adding a pier at $X/D = 6.0$ led to the formation of an additional local scour hole. Therefore, the scour hole was wider in the case of $X/D = 6.0$ than in other cases due to the combination of the pier scour hole and the abutment scour hole. This impact on d_{sa} was trivial in the case of $X/D \geq 3.0$ and in some cases of $X/D = 1.5$ (i.e., SCS1, SCR1, and SWR1). A separate scour hole around the pier was found when $X/D \geq 3.0$. However, when $X/D = 1.5$, the scour hole around the abutment changed, and a single large scour hole formed around both the pier and abutment instead of two separate scour holes.

Oben-Nyarko and Ettema (2011) used large-scale particle image velocimetry (LSPIV) images of flow and found that a relatively small amount of flow passed through the area between the pier and abutment when the pier was close to the abutment (e.g., $X/D = 1.5$). The discharge passing through the pier and abutment increased when the pier was located further away from the abutment. When the pier was close to the abutment ($X/D = 1.5$), the pier and abutment could act as a united obstacle to the flow and lead to a single large scour hole. Therefore, no separate scour hole formed around the pier.

3.8. Empirical equations for prediction of pier scour depth

Typical design practices suggest that individual scour components can be added together to calculate the overall scour depth for the combination of the pier and abutment (Hong and Abid, 2016). However, the joint interaction of these components in the main tests revealed that this method might overestimate d_{sp}. In addition, the overall scour depth estimation using typical design practices ignores the distance between the pier and abutment, which can significantly affect estimation accuracy. Table 1 shows that the sum of the maximum scour depths of a solitary pier and a solitary abutment largely overestimated d_{sp} or d_{sa}. Hence, the following equation was derived from the tests to estimate the scour depth around the pier when influenced by the abutment using the principle of superposition:

$$\frac{d_{sp}}{D} = \frac{d_{sp0}}{D} + \left| \frac{d_{sa0}}{D \tan \varphi} - \left(\frac{X}{D} + \frac{1}{2} \right) \right| \tan \varphi \qquad \frac{X}{D} \leq 6.0 \tag{3}$$

where φ is the angle of repose of the bed materials. Eq. (3) can estimate the maximum scour depth at a pier located at any distance X away from an abutment given d_{sp0}, d_{sa0}, and the angle of repose of the bed materials. The calculated values of the relative pier scour depth are given in Table 1. This equation was derived from the geometric relationship in the scour cross-section profile. Further details of this derivation are provided in Fig. A.4.

Fig. 11(a) shows a scatter plot of the measured d_{sp}/D versus the calculated d_{sp}/D using Eq. (3). The dashed lines represent the ±10% error band. Eq. (3) rationally estimated the scour depth within an acceptable range, and the errors of most calculated d_{sp}/D were less than 10%. The mean absolute error (*MAE*), root mean square error (*RMSE*), and coefficient of determination (R^2) were 0.30, 0.37, and 0.86, respectively. The scour process occurs layer by layer, and the scour profile is geometrically self-similar (Dey and Barbhuiya, 2005a). Thus, Eq. (3) can be used not only to estimate d_{sp} but also to calculate the scour depth at any time given the scour depths around a solitary pier and a solitary abutment at that time.

Comparison of Tables 1 and A.1 reveals that existing prediction formulas could lead to considerable errors in estimating the scour depth when the pier was within the interaction region of the abutment. Hence, Eq. (3), derived from the experiments, can be considered a better method with a high confidence level. The formulas use constant shape coefficients. Similarly, regression analysis was conducted on the results to derive the following equation that can predict the scour depth around a pier near an abutment according to the shape, type, and arrangement of the pier and abutment:

$$\frac{d_{sp}}{D} = K_{sa} K_{sp} \left[0.19 \left(\frac{X}{D} \right)^2 - \frac{1.8X}{D} + 6.2 \right] \tag{4}$$

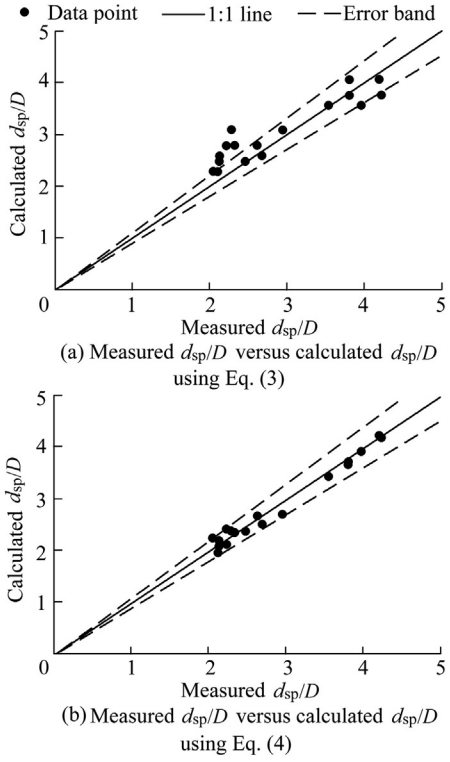

(a) Measured d_{sp}/D versus calculated d_{sp}/D using Eq. (3)

(b) Measured d_{sp}/D versus calculated d_{sp}/D using Eq. (4)

Fig. 11. Comparison between measured and calculated scour depths using Eqs. (3) and (4).

where K_{sa} is an abutment shape factor with $K_{sa} = 1.14$ for abutment W and $K_{sa} = 1.00$ for abutment C; and K_{sp} is a pier shape factor with $K_{sp} = 0.94$, 0.95, and 0.88 for piers S, G, and R, respectively. This equation accurately estimated d_{sp} in the vicinity of the abutment with $RMSE = 0.12$, $MAE = 0.10$, and $R^2 = 0.98$ (Fig. 11(b)). The advantage of Eq. (4) is that this equation can calculate the scour depth given the distance between the pier and abutment and their shapes. Table 1 shows the scour depth calculated by Eq. (4). The uncertainty and limitations of Eq. (4) are further described in Appendix A.

4. Conclusions

This study conducted laboratory tests and analysed the maximum scour depth and scour pattern in clear-water conditions, when piers and abutments with various shapes and layouts were combined. The flow streamline, velocity, bed shear stress, scour topography, and lateral scour hole cross-section were measured and analysed. The main conclusions are as follows: When a pier was located near an abutment, the flow characteristics around the pier changed, and primary vortices generated by the abutment led to a deeper and broader scour hole around the pier and abutment. High flow velocities appeared in the two regions upstream and left of the abutment and pier, which caused a wider scour hole. The presence of a pier in the vicinity of an abutment had a minor impact on the maximum scour depth around the abutment, although the scour hole volume increased by up to 87%. The maximum scour depth increased slightly when $X/D = 1.5$. The presence of a pier near an abutment significantly increased the scour depth around the pier. When the distance between the pier and abutment decreased, the maximum scour depth around the pier increased by up to 175% for $X/D = 1.5$. Using the principle of superposition of the scour depths around a solitary pier and around a solitary abutment, empirical equations were derived to accurately estimate the maximum scour depth at a pier adjacent to an abutment.

Declaration of competing interest

The authors declare no conflicts of interest.

Acknowledgements

The authors wish to acknowledge the editor and two anonymous reviewers for providing constructive comments, which substantially improved the quality of this article. The third author, Kourosh Behzadian, wishes to acknowledge support of the Royal Academy of Engineering through the Leverhulme Trust Research Fellowships.

Appendix A. Supplementary data

Supplementary data to this article can be found online at https://doi.org/10.1016/j.wse.2022.12.001.

References

Abid, I., 2017. Interaction of Pier, Contraction, and Abutment Scour in Clear Water Scour Conditions. Ph.D. Dissertation. Georgia Institute of Technology, Atlanta.

Chiew, Y.M., Melville, B.W., 1987. Local scour around bridge piers. J. Hydraul. Res. 25(1), 15−26. https://doi.org/10.1080/00221688709499285.

Chiew, Y.M., 1995. Mechanics of riprap failure at bridge piers. J. Hydraul. Eng. 121(9), 635−643. https://doi.org/10.1061/(ASCE)0733-9429, 1995)121:9(635.

Coleman, S.E., Lauchlan, C.S., Melville, B.W., 2003. Clear-water scour development at bridge abutments. J. Hydraul. Res. 41(5), 521−531. https://doi.org/10.1080/00221680309499997.

Dey, S., Barbhuiya, A., 2005a. Time variation of scour at abutments. J. Hydraul. Eng. 131(1), 11−23. https://doi.org/10.1061/(ASCE)0733-9429, 2005)131:1(11.

Dey, S., Barbhuiya, A., 2005b. Flow field at a vertical-wall abutment. J. Hydraul. Eng. 131(12), 1126−1135. https://doi.org/10.1061/(ASCE)0733-9429, 2005)131:12(1126.

Ettema, R., 1980. Scour at Bridge Piers. University of Auckland, Auckland.

Fael, C., Lança, R., Cardoso, A., 2016. Effect of pier shape and pier alignment on the equilibrium scour depth at single piers. Int. J. Sediment Res. 31(3), 244−250. https://doi.org/10.1016/j.ijsrc.2016.04.001.

Froehlich, D.C., 1988. Analysis of onsite measurements of scour at piers. In: Hydraulic Engineering: Proceedings of the 1988 National Conference on Hydraulic Engineering. ASCE, New York, pp. 534−539.

Guan, D., Chiew, Y.M., Wei, M., Hsieh, S.C., 2019. Characterization of horseshoe vortex in a developing scour hole at a cylindrical bridge pier. Int. J. Sediment Res. 34(2), 118−124. https://doi.org/10.1016/j.ijsrc.2018.07.001.

Hamill, L., 2011. Understanding Hydraulics. Macmillan International Higher Education, London.

Hong, S., 2005. Interaction of Bridge Contraction Scour and Pier Scour in a Laboratory River Model. M.S. Dissertation. Georgia Institute of Technology, Atlanta.

Hong, S., Abid, I., 2016. Physical model study of bridge contraction scour. KSCE J. Civ. Eng. 20(6), 2578−2585. https://doi.org/10.1007/s12205-015-0417-x.

Karami, H., Ardeshir, A., Behzadian, K., Ghodsian, M., 2011. Protective spur dike for scour mitigation of existing spur dikes. J. Hydraul. Res. 49(6), 809−813. https://doi.org/10.1080/00221686.2011.625166.

Khajeh, S.B.M., Vaghefi, M., 2020. Investigation of abutment effect on scouring around inclined pier at a bend. J. Appl. Water Eng. Res. 8(2), 125−138. https://doi.org/10.1080/23249676.2020.1761898.

Kirkgöz, M.S., Ardiçlioğlu, M., 1997. Velocity profiles of developing and developed open channel flow. J. Hydraul. Eng. 123(12), 1099−1105. https://doi.org/10.1061/(ASCE)0733-9429, 1997)123:12(1099.

Kumcu, S., Kokpinar, M., Gogus, M., 2014. Scour protection around vertical-wall bridge abutments with collars. KSCE J. Civ. Eng. 18(6), 1884−1895. https://doi.org/10.1007/s12205-014-0245-4.

Lamb, R., Garside, P., Pant, R., Hall, J.W., 2019. A probabilistic model of the economic risk to britain's railway network from bridge scour during floods. Risk Anal. 39(11), 2457−2478. https://doi.org/10.1111/risa.13370.

Mays, L.W., 2001. Stormwater Collection Systems Design Handbook. McGraw-Hill Education, New York.

Melville, B.W., Raudkivi, A.J., 1977. Flow characteristics in local scour at bridge piers. J. Hydraul. Res. 15(4), 373−380. https://doi.org/10.1080/00221687709499641.

Melville, B.W., 1992. Local scour at bridge abutments. J. Hydraul. Eng. 118(4), 615−631. https://doi.org/10.1061/(ASCE)0733-9429, 1992)118:4(615.

Melville, B.W., 1997. Pier and abutment scour: Integrated approach. J. Hydraul. Eng. 123(2), 125−136. https://doi.org/10.1061/(ASCE)0733-9429, 1997)123:2(125.

Melville, B.W., Coleman, S.E., 2000. Bridge Scour. Water Resources Publications, Colorado.

Melville, B.W., Yang, Y., Xiong, X., Ettema, R., Nowroozpour, A., 2021. Effects of streamwise abutment length on scour at riprap apron-protected setback abutments in compound channels. J. Hydraul. Eng. 147(3), 04021003. https://doi.org/10.1061/(ASCE)HY.1943-7900.0001860.

Oben-Nyarko, K., Ettema, R., 2011. Pier and abutment scour interaction. J. Hydraul. Eng. 137(12), 1598−1605. https://doi.org/10.1061/(ASCE)HY.1943-7900.0000446.

Pasupuleti, L.N., Timbadiya, P.V., Patel, P.L., 2022. Flow field measurements around isolated, staggered, and tandem piers on a rigid bed channel. Int. J. Civ. Eng. 20, 569−586. https://doi.org/10.1007/s40999-021-00678-w.

Pizarro, A., Manfreda, S., Tubaldi, E., 2020. The science behind scour at bridge foundations: A review. Water 12(2), 374. https://doi.org/10.3390/w12020374.

Rahimi, E., Qaderi, K., Rahimpour, M., Ahmadi, M.M., Madadi, M.R., 2021. Scour at side by side pier and abutment with debris accumulation. Mar. Georesour. Geotechnol. 39(4), 459−470. https://doi.org/10.1080/1064119X.2020.1716122.

Richardson, E.V., Davis, S.R., 2001. Evaluating scour at bridges. In: Hydraulic Engineering Circular No. 18. Department of Transportation, Washington D.C.

Saha, R., Lee, S.O., Hong, S.H., 2018. A comprehensive method of calculating maximum bridge scour depth. Water 10(11), 1572. https://doi.org/10.3390/w10111572.

Sheppard, D., Miller, W., 2006. Live-bed local pier scour experiments. J. Hydraul. Eng. 132(7), 635−642. https://doi.org/10.1061/(ASCE)0733-9429, 2006)132:7(635.

Sheppard, D., Melville, B., Demir, H., 2014. Evaluation of existing equations for local scour at bridge piers. J. Hydraul. Eng. 140(1), 14−23. https://doi.org/10.1061/(ASCE)HY.1943-7900.0000800.

Yang, Y., Xiong, X., Melville, B., Sturm, T., 2020. Flow redistribution at bridge contractions in compound channel for extreme hydrological events and implications for sediment scour. J. Hydraul. Eng. 147(3), 04021005. https://doi.org/10.1061/(ASCE)HY.1943-7900.0001861.

Zhang, W., Wang, L., Melville, B.W., Guan, D., Whittaker, C.N., Shamseldin, A.Y., 2021. Characteristics of the flow field within a developing scour hole at a submerged weir. J. Hydraul. Res. 60(2), 283−294. https://doi.org/10.1080/00221686.2021.1944928.